Imaging of quantum array structures with coherent and partially coherent diffraction

I. A. Vartanyants*† and I. K. Robinson

Department of Physics, University of Illinois, 1110 West Green Street, Urbana, IL 61801, USA.
E-mail: vartaniants@mrl.uiuc.edu

Recent achievements in experimental and computational methods open the possibility of measuring and inverting the diffraction pattern from a finite object of submicrometer size. In this paper the possibilities of such experiments for two-dimensional arrays of quantum dots are discussed. The diffraction pattern corresponding to coherent and partial coherent illumination of a sample was generated. Test calculations based on the iterative algorithms were applied to reconstruct the shape of the individual islands in such a quantum structure directly from its diffraction pattern. It is demonstrated that, in the case of coherent illumination, the correct shape and orientation of an individual island can be obtained. In the case of partially coherent illumination, the correct shape of the particle can be obtained only when the coherence of the incoming beam is reduced to match the size of the island.

Keywords: X-ray coherent diffraction; quantum dot structure; imaging.

1. Introduction

Quantum structures (quantum wires and quantum dots) are important elements of modern nanophysics and nanotechnology. Confinement of the electron wavefunction to dimensions of the order of 10 to 100 nm, which is less than the electron's mean free path, drastically changes both energy levels and the density of states. On the one hand this provides a unique opportunity to test quantum mechanical concepts, and on the other provides wide opportunities for applications in the optoelectronics and semiconductor industry (Bimberg *et al.*, 1999). Different methods have been proposed for growing such nanostructures. One common approach is the self-organized growth technique when nanostructures are spontaneously formed during the deposition of strained epitaxic layers. This technique can produce very small structures with a high lateral density that can be grown within a short time. Unfortunately the control of the growth process during self-organization is difficult, as size, shape and composition depend sensitively on several parameters. At the same time it is clear that the electronic properties of nanodevices based on quantum structures are first of all determined by their shape.

Characterization techniques are required both for the studies of the fundamental physical properties as well as for the optimization of growth parameters of quantum structures. Surface atomic force microscopy (AFM) (Springholz *et al.*, 1998; Lee *et al.*, 2001) and scanning tunnelling microscopy (STM) (Medeiros-Ribeiro *et al.*, 1998; Marquez *et al.*, 2001) are commonly used for characterization of the shape and the size of the quantum structures, but only when they are present on an open surface. For practical applications, however, the quantum structures have to be overgrown. It is known that this is often accompanied by a considerable change of the size and shape of the nanostructures due to interdiffusion and segregation (Sutter & Lagally, 1998; Mateeva *et al.*, 1999). Hence, methods are required that allow for the characterization of buried quantum dots. This is often done by transmission electron microscopy (TEM) (Liu, Gibson *et al.*, 2000; Walther *et al.*, 2001) and cross-sectional STM (Eisele *et al.*, 1999; Liu, Tersoff *et al.*, 2000). Although these methods often give 'direct images', they are only two-dimensional and the applications are often limited by elaborate sample preparation.

Owing to their high penetration depth, X-rays are favorable in the study of buried crystal structures. First of all, X-ray methods are non-destructive and, secondly, different X-ray scattering and diffraction techniques can provide complementary information about the shape, size, deformation and composition of the quantum structures. As was shown in a series of papers, the average shapes, sizes and correlation lengths can be effectively obtained by grazing-incidence small-angle X-ray scattering (GISAXS) (Schmidbauer *et al.*, 1998; Stangl *et al.*, 2000; Holy *et al.*, 2001). Composition and strain can be investigated by X-ray diffraction using coplanar geometry (XRD) (Shen *et al.*, 1996; Darhuber *et al.*, 1997; Wiebach *et al.*, 2000) or in grazing-incidence diffraction (GID) (Steinfort *et al.*, 1996; Kegel *et al.*, 2001). These X-ray scattering techniques have been widely applied to the study of quantum structures (Holy *et al.*, 1999; Stangl *et al.*, 2002). Already in the early publications (Shen *et al.*, 1993; Salditt *et al.*, 1994) the questions of coherence length of the incoming beam and diffraction contrast from periodic quantum structures were addressed. These ideas were even used for a detailed study of the partial coherence of the synchrotron beam (Lin *et al.*, 1998). In all these methods, however, contrary to imaging methods discussed before, *average* information is obtained. Furthermore, the most valuable information (shape, size and deformation) can be obtained only indirectly by comparing results of the experiment with simulated diffraction patterns obtained from models. In this paper we want to discuss the possibilities of combining diffraction methods with a new lensless imaging technique for investigation of quantum structures.

Recently it was shown that if a sample of finite size is coherently illuminated and its diffraction pattern is measured with a frequency that is two times higher than the Nyquist frequency, then (in dimensions higher than one) it can be uniquely inverted to give a real-space image of the sample (Miao *et al.*, 1999, 2002). It was shown that, by illuminating just one crystalline particle of submicrometer size with a coherent X-ray beam, the shape of this particle can be obtained in two dimensions and three dimensions (Robinson *et al.*, 2001; Williams *et al.*, 2003). An oversampling method was also tested on a computer-generated two-dimensional crystal structure and repeated motif without orientational regularity (Miao & Sayre, 2000). However, under the present state of the experimental capabilities, owing to a variety of reasons, it is difficult to perform such an experiment on quantum structures. First of all, it is difficult to illuminate just one quantum dot even using focusing techniques because the size and the distance separation between typical quantum dots is on the nanometer scale. Secondly, even using the high flux of third-generation X-ray synchrotron sources, the signal obtained just from scattering by one quantum dot will be below a measurable level. So, instead of illuminating one quantum dot the favorable strategy might be coherent illumination of a finite array of quantum dots. In this case both problems stated above could be overcome. Nanometer focusing of the incoming beam is not necessary and the signal scattered by a finite number of the dots will be measurable at synchrotron sources. The ideas are quite general and in principle can be applied to different diffraction techniques not limited to X-rays. For example, the same approach can also be useful for imaging by electron beams. As was demonstrated in a recent experiment (Zuo *et al.*, 2003), if the diffraction pattern is recorded using TEM (without the use of imaging

† On leave from Institute of Crystallography RAS, Leninsky pr. 59, 117333 Moscow, Russia.

 © 2003 International Union of Crystallography • Printed in Great Britain – all rights reserved

lenses for converting the image from reciprocal to real space), atomic resolution can be successfully obtained by inversion of the oversampled data. In this paper we would like to discuss the feasibility of this technique for imaging quantum structures by computer simulations.

Quite a different approach, proposed recently by Szöke (2001) for biological crystals, can also be used for imaging quantum structures as test objects. If, instead of a highly coherent beam, the sample is illuminated by an incoherent beam with coherence length approximately equal to the distance between the molecules, then the diffraction pattern just from one molecule will be recorded. The intensity recorded on the detector will be an incoherent sum of coherent diffraction patterns from all identical molecules illuminated by this strongly incoherent beam. Here we are not discussing different approaches of preparing such an incoherent beam, which can be rather difficult, but will show by computer simulations the advantages and disadvantages of this approach for quantum structure imaging.

The paper is organized as follows. In §2 we will discuss imaging of quantum structures with coherent illumination, in §3 imaging with an incoherent beam, and in the last section we will give the conclusion and discussion of the results obtained.

2. Imaging of quantum structures with coherent beams

Here, for purposes of clarity, we will consider the case of the in-line geometry when a two-dimensional detector (such as a CCD camera) is positioned downstream from the sample and the array of quantum dots (QD) is perpendicular to the beam propagation direction. With the same purpose we will consider a regular array of QDs arranged in a two-dimensional lattice, which often occurs in practice owing to self-organization during growth (Stangl *et al.*, 2002). The shape of the QDs will be taken in the form of triangular pyramids, terminated by {100} side facets.

In the case of coherent illumination of such an array of QDs, the electron density $p(\mathbf{r})$ can be written in the following form,

$$p(\mathbf{r}) = S(\mathbf{r})\big[s_z(\mathbf{r}) \otimes p_\infty(\mathbf{r})\big], \tag{1}$$

where $S(\mathbf{r})$ is the shape of the coherently illuminated area on the sample, $s_z(\mathbf{r}) = \int \mathrm{d}z\, s(\mathbf{r}, z)$ is the projection of the shape function (or electron density) of one island $s(\mathbf{r}, z)$ on the surface plane, $p_\infty(\mathbf{r}) = \sum_n \delta(\mathbf{r} - \mathbf{r}_n)$ is a periodic function defining a two-dimensional lattice, $\otimes$ is a convolution sign and $\mathbf{r}$ is a two-dimensional coordinate vector in the plane of the sample surface. The scattered amplitude in the kinematic approximation is just the Fourier transform (FT) of this electron density,

$$A(\mathbf{q}) = \int p(\mathbf{r}) \exp(i\mathbf{q}\mathbf{r})\, \mathrm{d}\mathbf{r}, \tag{2}$$

where $\mathbf{q}$ is a two-dimensional scattering vector. The intensity measured at the detector is the square modulus of this amplitude with the necessary loss of the phase.

In the case of the perfect two-dimensional lattice considered here it is possible to show that this amplitude is equal to

$$A(\mathbf{q}) = \sum_n s_z(\mathbf{h}_n) S(\mathbf{q} - \mathbf{h}_n), \tag{3}$$

where $s_z(\mathbf{q})$ is the FT of $s_z(\mathbf{r})$, the shape function of the island, $S(\mathbf{q})$ is the FT of $S(\mathbf{r})$, the coherently illuminated area, and $\mathbf{h}_n = 2\pi\mathbf{H}_n$, $\mathbf{H}_n$ being the two-dimensional reciprocal-lattice vectors. When the size of the QD is much smaller then the distance between QDs which are themselves much smaller than the coherently illuminated area, the scattered intensity can be written as

$$I_{\mathrm{coh}}(\mathbf{q}) = |A(\mathbf{q})|^2 = \sum_n |s_z(\mathbf{h}_n)|^2 |S(\mathbf{q} - \mathbf{h}_n)|^2 + \text{ cross terms}. \tag{4}$$

This equation has a simple meaning. The leading term in this expression describes the diffraction pattern from an array of QDs which is a periodic array of the Bragg peaks with the symmetry of the two-dimensional lattice of QDs. Each Bragg peak will be smeared by the distribution $|S(\mathbf{q})|^2$ with a half-width of about $2\pi/L$, where L is the size of the coherently illuminated area. In addition, the whole pattern will be modulated by the FT of the shape function corresponding to one island, $|s_z(\mathbf{h}_n)|^2$. There will be intensity modulation between the Bragg peaks because of a small cross-term contribution in (4). Our goal will be to invert this diffraction pattern in order to reconstruct the electron density $p(\mathbf{r})$, (1). It is important here that the diffraction pattern has to be recorded continuously including all information between the Bragg peaks measured over a wide reciprocal space region.

We generated an array of QDs of pyramid shape shown in Fig. 1(*a*). The edge of each pyramid was 40 pixels in size (a magnified image of one pyramid is shown in Fig. 1*b*). The two-dimensional array was generated by two unit vectors, $\mathbf{a}_1 = (64, 0)$ and $\mathbf{a}_2 = (32, 55)$, giving rise to the hexagonal structure shown in Fig. 1(*a*). It was then assumed that this array of QDs was coherently illuminated by a beam with a circular shape and radius $L = 150$ pixels, ramping smoothly to zero over ten more pixels. The diffraction pattern corresponding to this array of QDs was calculated as a discrete FT and is shown in Fig. 1(*c*).

The diffraction pattern reproduces all the main features that we would expect. First of all the regular hexagonal array of Bragg spots is clearly observed in the figure. The size of each Bragg spot is defined by the size of the coherently illuminated area and has a circular shape.

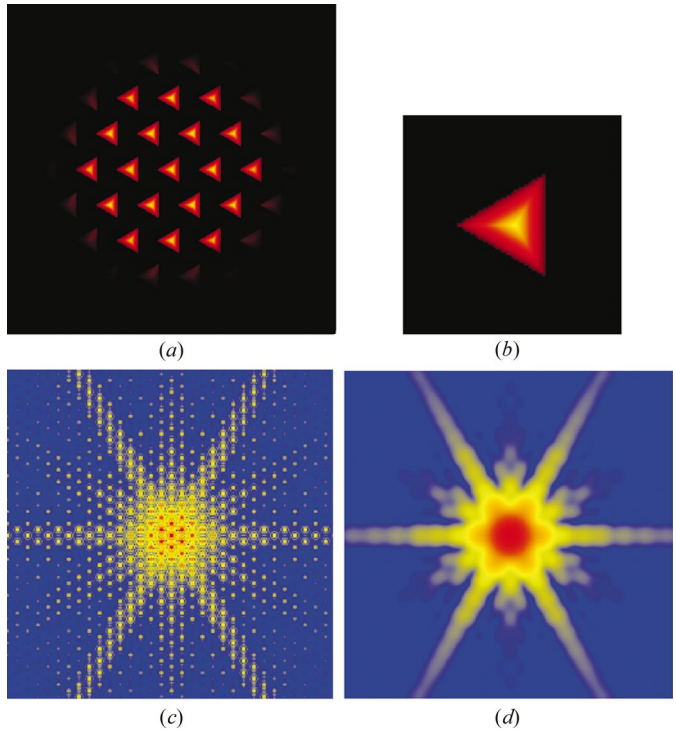

Figure 1
(*a*) Computer simulated two-dimensional array of quantum dots of pyramid shape. The total size of the array is 512 × 512 pixels. (*b*) Magnified image of an individual island. (*c*) Diffraction intensity corresponding to the two-dimensional array of QDs in (*a*). The central 255 × 255 pixels of the diffraction pattern are shown. (*d*) Diffraction intensity corresponding to an individual island in (*b*).

The whole intensity is modulated by the shape of the FT of a single QD (Fig. 1*d*). Typical features of this diffraction pattern consist of strong flares of intensity originating from scattering from each facet (Vartanyants & Robinson, 2001). The diffraction pattern does not contain any interference fringes because there are no parallel facets on a triangular-shape pyramid [contrary to interference fringes from real Au particles, where such fringes were observed (Robinson *et al.*, 2001; Williams *et al.*, 2003)].

If the typical size of the island in the two-dimensional array is about 50 nm, then the reciprocal-space region shown in Figs. 1(*c*) and 1(*d*) will correspond to $\Delta Q \simeq 2.22\ \mathrm{nm}^{-1}$ with the pixel size $\Delta q = 0.0087\ \mathrm{nm}^{-1}$. This is more then an order of magnitude bigger than the resolution obtained in recent coherent X-ray diffraction experiments (Robinson *et al.*, 2001; Williams *et al.*, 2003). The coherently illuminated region assumed in our calculations will be $L = 0.21\ \mu\mathrm{m}$.

The calculated diffraction pattern was used to reconstruct the initial two-dimensional lattice of QDs. In order to invert the intensity distribution shown in Fig. 1(*c*) we used an iterative approach first proposed by Gerchberg & Saxton (1972) and then further developed by Fienup (1982). It is important for this method of phase retrieval that no starting model is used for fitting the data. In the first step the missing phases are taken as a pseudo-random set and are combined with the amplitudes in reciprocal space. Then a FT is applied back and forth with specific constraints used in both real and reciprocal space. To test the reproducibility, the calculations were repeated with another set of starting random phases. The following constraints were applied. In reciprocal space the calculated amplitude on each iteration step was replaced by the Fourier amplitude $I(\mathbf{q})^{1/2}$, (4). In real space, assuming relaxed islands without strain, we can take as a powerful constraint that the electron density $p(\mathbf{r})$, (1), has to be real and positive. One further important parameter for reconstructing the image from the diffracted intensity is to define the support region. In our case (Fig. 2*a*) we took it as a product of two functions. One of them was the function $S(\mathbf{r})$ defining the coherently illuminated region and the other was a lattice function defining the position of each individual island in the lattice. In the real experiment such a function can be estimated from the symmetry of the Bragg spots in the diffracted pattern. The size of each small quadrangle can be taken as a little bit bigger then the actual size of the particle (which can also be estimated from the shape of the diffraction pattern) allowing small shifts of the position of individual islands from ideal lattice sites. Such a constraint is in fact similar to the 'atomicity' projection constraint proposed recently (Elser, 2003) for crystallographic reconstruction with atomic resolution. Using such a support provides us with a high oversampling ratio ($\sigma = S_{\mathrm{FFT}}/S_{\mathrm{support}} \gg 2$) as is important for the convergence of the algorithm (Millane, 1996; Miao *et al.*, 1998). To avoid stagnations we used an alternation of two algorithms: error reduction (ER) and hybrid input–output (HIO) (Fienup, 1982; Millane & Stroud, 1997), having about 1000 cycles for each set of random phases. A detailed description of these algorithms and actual parameters used in reconstruction was given in our previous publication (Vartanyants & Robinson, 2001).

Two typical reconstructed images corresponding to the lowest value of the error metric are shown in Fig. 2. The image presented in Fig. 2(*b*) gives an exact reconstruction of the QD array. It not only gives the correct position of each island that is defined by our choice of support region in the form of a two-dimensional lattice but also gives the correct orientation of each island. The corresponding diffraction pattern is presented in Fig. 2(*c*). It has all the features present in the initial diffraction pattern (Fig. 1*c*). In Fig. 2(*d*) we also present another result of reconstruction that often appears in the fitting. The position of each island is again reproduced correctly; however, the shape of the individual island is not reconstructed properly. The origin of the problem lies in the inversion symmetry of the diffraction pattern (Fig. 1*c*). The positive electron density of Fig. 1(*a*) rotated through 180° will produce the same diffraction pattern as in Fig. 1(*c*). So, the reconstructed image shown in Fig. 2(*d*) is a mixture of these two twin images. This is a well known source of frustration of these iterative methods (Fienup & Wackerman, 1986). Our test calculations have shown that for 20 independent fits with different starting phases the correct image is obtained typically for the two lowest values of the error metrics. The next best result was usually a superposition of two twin images.

We also checked how stable the reconstruction procedure was to the exact matching of the original and constraint lattice functions (Figs. 1*a* and 2*a*). Our calculations have shown that mismatch of the lattice vectors by as much as a few pixels still gives a good reconstruction image with a slight blurring that increases with the mismatch. The most important restriction here is that the shifted position of each individual quadrangle in Fig. 2(*a*) would still cover the position of the QDs in Fig. 1(*a*).

3. Imaging with partially coherent beams

In the previous section we were considering the coherent illumination of the two-dimensional lattice containing a finite number of QDs. Now we will investigate how imaging of an individual island can change if a partially coherent incoming beam is considered. The general properties of partially coherent radiation are well established in the optics literature (Goodman, 1985; Born & Wolf, 1999; Mandel & Wolf, 1995). Vartanyants & Robinson (2001) showed that partially coherent X-ray illumination of an object with electron density $p(\mathbf{r})$, (1), gives a far-field intensity distribution on the detector,

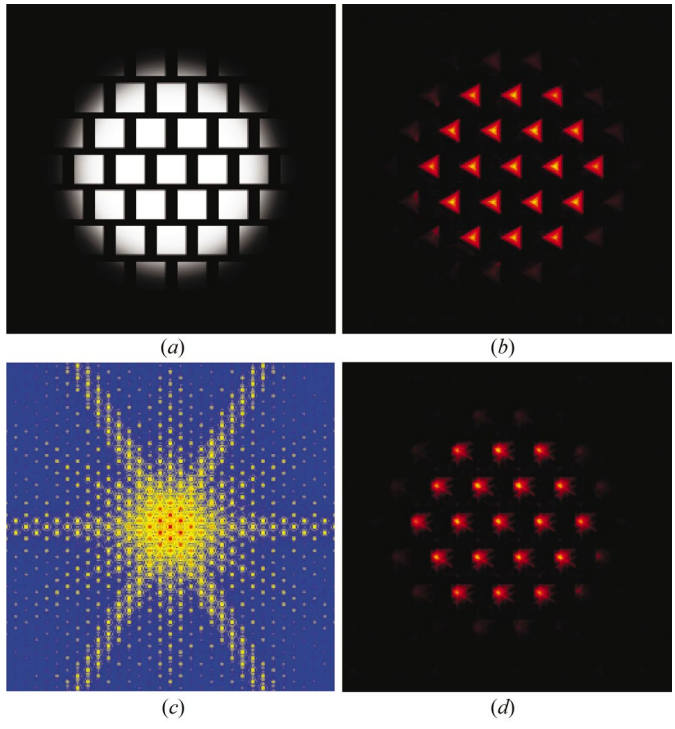

Figure 2
(*a*) Support used for reconstruction of the quantum dot array. (*b*) Image of the quantum dot array reconstructed from the diffraction pattern shown in Fig. 1(*c*). (*c*) Diffraction intensity corresponding to the reconstructed image (*b*). (*d*) The real-space fit as a result of superposition of two twin images.

$$I(\mathbf{q}) = \iint \mathrm{d}\mathbf{r}\,\mathrm{d}\mathbf{r}'\,p(\mathbf{r})p(\mathbf{r}')\,J_{\rm in}(\mathbf{r},\mathbf{r}')\exp[-i\mathbf{q}(r-r')], \quad (5)$$

where $J_{\rm in}(\mathbf{r},\mathbf{r}')$ is the mutual intensity function (MIF) of the beam incoming on the sample. Expression (5) is valid if quasimonochromatic conditions are satisfied, which means in this kind of experiment that time delays for X-ray propagation in a sample $\Delta\tau = (l_r - l_{r'})/c$ are much less than coherence times, $\Delta\tau \ll \tau_c = l_c/c$. The MIF $J_{\rm in}(\mathbf{r},\mathbf{r}')$ describes the statistical properties of the incoming wavefield as a correlation function between two complex scalar values of the electric field, $E_{\rm in}(\mathbf{r}_1, t)$ and $E_{\rm in}(\mathbf{r}_2, t)$, at different points $\mathbf{r}_1$ and $\mathbf{r}_2$ in space at the same time t. It is usual also to introduce the normalized MIF,

$$\mu_{\rm in}(\mathbf{r}_1,\mathbf{r}_2) = J_{\rm in}(\mathbf{r}_1,\mathbf{r}_2)/\left[I_{\rm in}(\mathbf{r}_1)I_{\rm in}(\mathbf{r}_2)\right]^{1/2}, \quad (6)$$

which is known as the complex coherence factor (CCF), and $I_{\rm in}(\mathbf{r}_1)$ and $I_{\rm in}(\mathbf{r}_2)$ are the intensity values of the incoming beam at points $\mathbf{r}_1$ and $\mathbf{r}_2$, respectively.

It was shown in our previous paper (Vartanyants & Robinson, 2003) that in general the shape of the CCF (6) can be very complicated owing to scattering from any optics present on the beamline where experiments are performed. Below we will consider a Gaussian form for the CCF,

$$\mu_{\rm in}(\mathbf{r}-\mathbf{r}') = \exp\left[-(\mathbf{r}-\mathbf{r}')^2/2l_{\rm coh}^2\right], \quad (7)$$

where $l_{\rm coh}$ is the transverse coherence length. This expression for the CCF will be an exact far-field solution according to the van Cittert–Zernike theorem (Goodman, 1985; Mandel & Wolf, 1995) for an incoherent source with Gaussian distribution of intensity. If the half-width of this intensity distribution in both directions is given by σ then the transverse coherence length $l_{\rm coh}$ in (7) is equal to $l_{\rm coh} = \lambda L_1/(2\pi\sigma)$, where λ is the wavelength of the incoming beam and L_1 is the distance from the source to the object.

Expression (5) can be written equivalently in the following form (Vartanyants & Robinson, 2001),

$$I(\mathbf{q}) = \int \mathrm{d}\mathbf{r}\;\varphi_{11}(\mathbf{r})\mu_{\rm in}(\mathbf{r})\exp(-i\mathbf{q}\cdot\mathbf{r}), \quad (8)$$

where

$$\varphi_{11}(\mathbf{r}) = \int \mathrm{d}\mathbf{r}'\,p(\mathbf{r}')p(\mathbf{r}'+\mathbf{r}) \quad (9)$$

is the autocorrelation function of the electron density $p(\mathbf{r})$. Using the convolution theorem, the scattered intensity (8) can be expressed in terms of $I_{\rm coh}(\mathbf{q})$, (4),

$$I(\mathbf{q}) = I_{\rm coh}(\mathbf{q}) \otimes \mu_{\rm in}(\mathbf{q}) = \left|A(\mathbf{q})\right|^2 \otimes \mu_{\rm in}(\mathbf{q}), \quad (10)$$

where $\mu_{\rm in}(\mathbf{q})$ is the FT of the CCF (6). Now, substituting the expression for $A(\mathbf{q})$, (3), we obtain the following result for the diffracted intensity from a two-dimensional array of QDs in the case of partially coherent illumination,

$$I(\mathbf{q}) = \sum_n |s_z(\mathbf{h}_n)|^2\left[|S(\mathbf{q}-\mathbf{h}_n)|^2 \otimes \mu_{\rm in}(\mathbf{q})\right] + \text{cross terms}. \quad (11)$$

Assuming a Gaussian shape for the CCF $\mu_{\rm in}(\mathbf{r})$, (7), we will also have a Gaussian distribution for $\mu_{\rm in}(\mathbf{q})$ in the reciprocal space with a typical length $q_{\rm coh} \simeq 2\pi/l_{\rm coh}$. In the case of coherent illumination, $l_{\rm coh} \gg L$, where L is the typical size of the illuminated part of the sample and $q_{\rm coh} \ll q_L = 2\pi/L$. In this limit, the FT of the CCF $\mu_{\rm in}(\mathbf{q})$ can be replaced by a delta function, $\mu_{\rm in}(\mathbf{q}) \rightarrow \delta(\mathbf{q})$. Substituting this into (11) will immediately give the coherent limit of (4), when the intensity distribution around each two-dimensional Bragg point is given by q_L.

If instead the coherence length $l_{\rm coh}$ is decreased, this will lead to an increase of $q_{\rm coh}$ in reciprocal space. When $l_{\rm coh}$ reaches the size L owing to convolution in equation (11) we will have an approximately twice as broad distribution in the reciprocal space around each Bragg peak. If we further decrease the coherence length but still keep it larger than the two-dimensional period of the QD lattice, then in (11) we will still have a periodic distribution of intensity corresponding to each Bragg position but with an increased width of each peak that will still be determined by the coherence length. Continuing this process, we will finally come to the situation where the coherence length will be less than the separation between the islands in the QD structure, but still bigger than the size of one individual island. In reciprocal space we expect a continuous non-periodic distribution of intensity with a shape given by the FT of an individual island, $|s_z(\mathbf{q})|^2$.

Our special interest in this work was to test the idea of Szöke (2001) mentioned in the introduction to understand what kind of image of a quantum structure can be obtained by the inversion of diffraction patterns for the different values of the transverse coherence length $l_{\rm coh}$. For this purpose we generated a different array of QDs, shown in Fig. 3(*a*). As in our previous example (Fig. 1), it consists of a two-dimensional array of pyramids but in this case with a square shape. The symmetry of the two-dimensional lattice was given by the lattice unit vectors $\mathbf{a}_1 = (60, 0)$ and $\mathbf{a}_2 = (60, 34)$. The shape of an individual island is shown in Fig. 3(*b*), the FT of the two-dimensional array of QDs is shown in Fig. 3(*c*), and the FT of an individual island is shown in Fig. 3(*d*). The diffraction pattern in Fig. 3(*c*) consists of an array of small individual Bragg spots with intensity smeared in the vertical and horizontal directions. The smearing originates from truncation of the two-dimensional lattice on each side of the sample. The width of each individual Bragg spot is much narrower than in the previous example (Fig. 1*c*) because the coherently illuminated area in the latter case is much larger. Like in the previous example, the overall modulation of the diffraction pattern is clearly observed by the shape of the FT of the individual island (Fig. 3*d*).

On the left-hand panels of Fig. 4, three different CCFs are shown for the incoming X-ray beam with reduced coherence length.

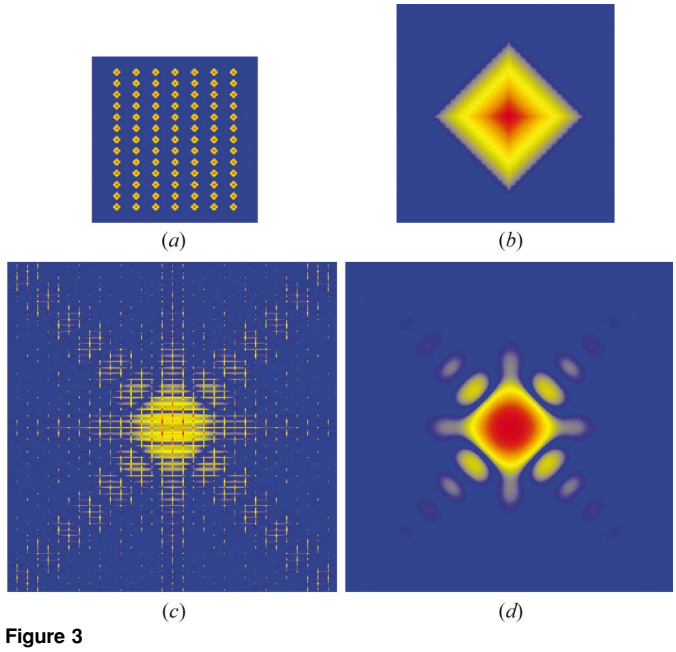

Figure 3
(*a*) Computer simulated two-dimensional array of quantum dots of pyramid shape used for the tests of the partial coherence effects. The total size of the array is 512 × 512 pixels. (*b*) Magnified image of an individual island. (*c*) Diffraction intensity corresponding to two-dimensional array of quantum dots in (*a*). The central 255 × 255 pixels of the diffraction pattern are shown. (*d*) Diffraction intensity corresponding to an individual island in (*b*).

According to (7), we assumed a Gaussian shape for the incoming CCF $\mu_{in}(\mathbf{r})$. Three different cases are shown for l_{coh} = 128, 64 and 31 pixels (Figs. 4*b*, 4*c* and 4*d*, respectively). The right-hand panels show the corresponding diffraction patterns (Figs. 4*f*, 4*g* and 4*h*), calculated according to equations (5) and (8). These patterns produce the general behavior that was predicted by the analysis of (11). The first trend is the increasing size of the Bragg spots, which have approximately a circular shape and a half-width of $\sim 2\pi/l_{coh}$. In the extreme case of a very small coherence length, l_{coh} = 31 pixels, the Bragg spots are hardly visible and the diffraction pattern becomes similar to the continuous diffraction pattern of an individual island (Fig. 3*d*). This behavior is also clearly observed from the central cross section of the diffraction patterns shown in Fig. 5.

We applied the iteration algorithm described in the previous section with the hope of reconstructing the shape of individual islands. The support region was taken in the form of a small square of size 35 × 35 pixels. Applying this algorithm we obtained the reconstructed images presented in Fig. 6. It is clearly seen from this figure that when the coherence length is large the reconstructed image resembles the correlation function $\varphi_{11}(\mathbf{r})$, (9) (Fig. 6*a*). When the coherence length is reduced, the number of copies surrounding the central particle is also reduced (Figs. 6*b* and 6*c*). Finally, in the limit of very small coherence lengths (about the size of an individual island), the reconstructed image contains only one bright reconstructed

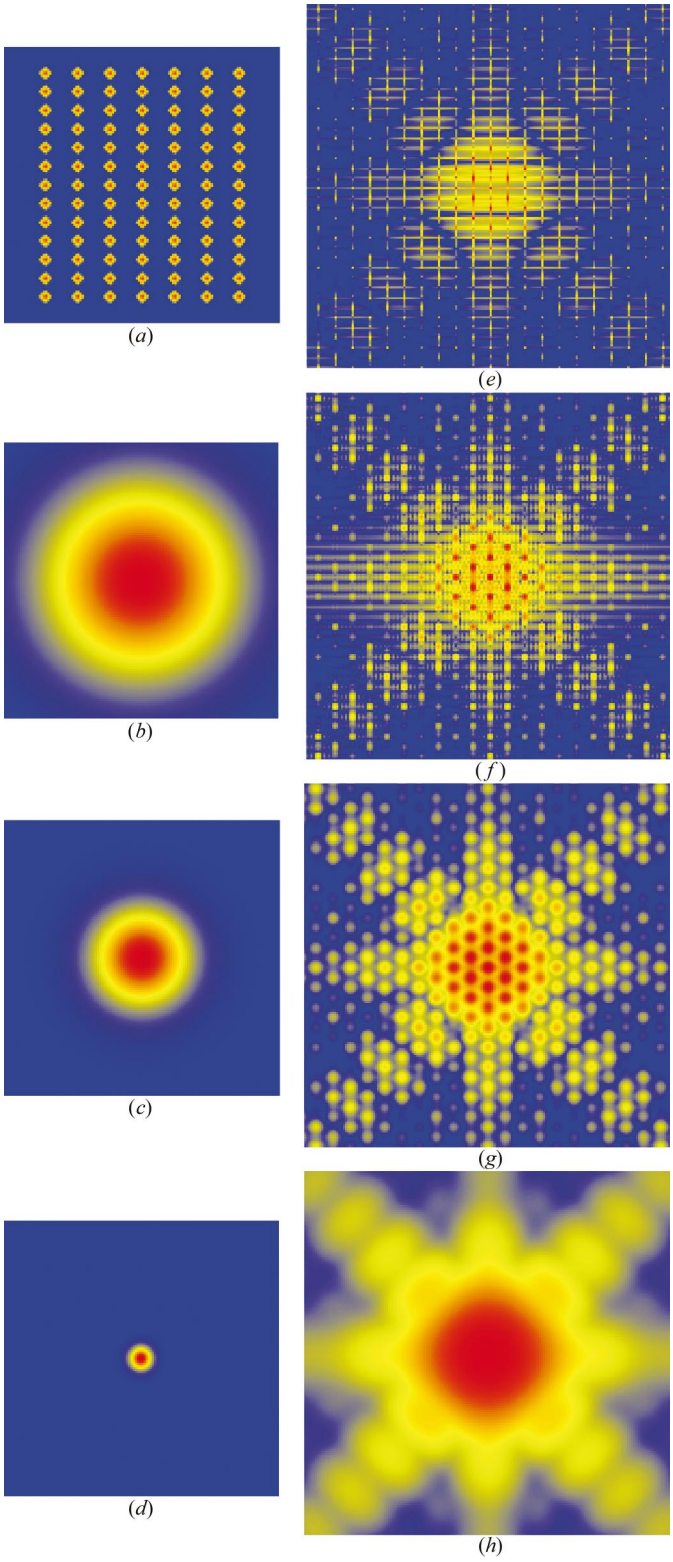

Figure 4
Complex coherence factor $\mu_{in}(\mathbf{r})$ (left-hand panel) used for calculation of diffraction intensity patterns (right-hand panel). For comparison, in the top row we show the case of coherent illumination. The values of the coherence lengths in the other rows are, from top to bottom, l_{coh} = 128, 64 and 31 pixels.

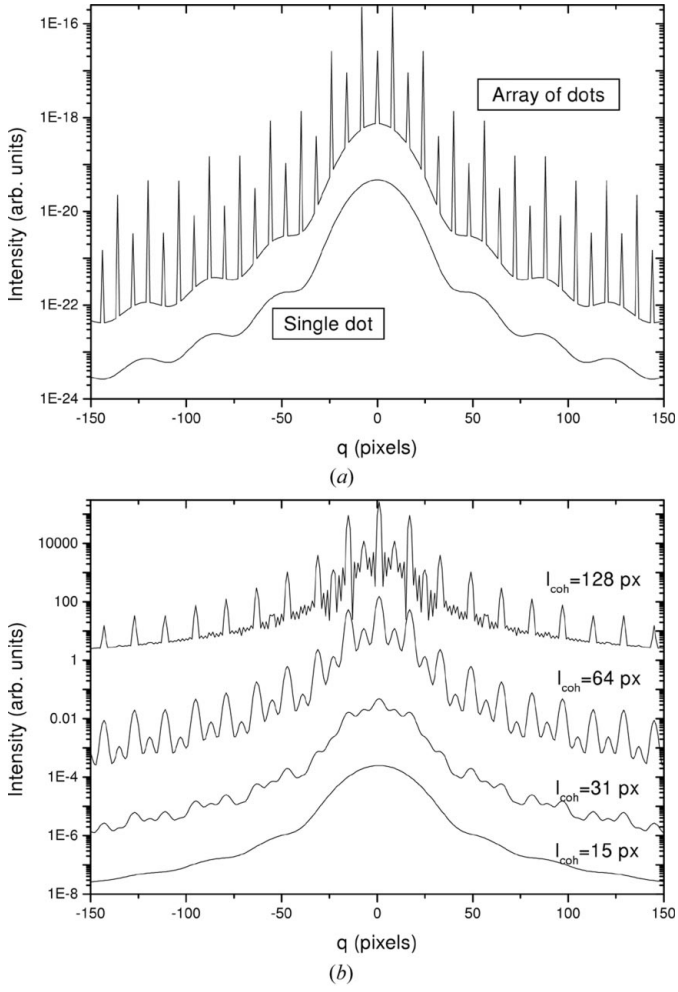

Figure 5
The equatorial cross section of the diffraction patterns from Figs. 3 and 4. (*a*) Coherent illumination of the two-dimensional array of quantum dots and individual island from Figs. 3(*c*) and 3(*d*). (*b*) Partially coherent illumination of the two-dimensional array of quantum dots with coherent lengths l_{coh} = 128, 64, 31 and 15 pixels from Fig. 4.

particle in the middle of an array (Fig. 6*d*). These results are understood to arise from using a single support instead of an array.

The average shape of the individual island can already be distinguished in the images with large coherence length (Figs. 6*e*, 6*f* and 6*g*); however, the quality deteriorates with reduced coherence. Finally, when the coherence length reaches the size of the particle the image quality improves and resembles the correct shape (Fig. 6*h*). Comparison of this image with the image of the original particle (Fig. 3*b*) shows that some small variations of density have been introduced inside the particle.

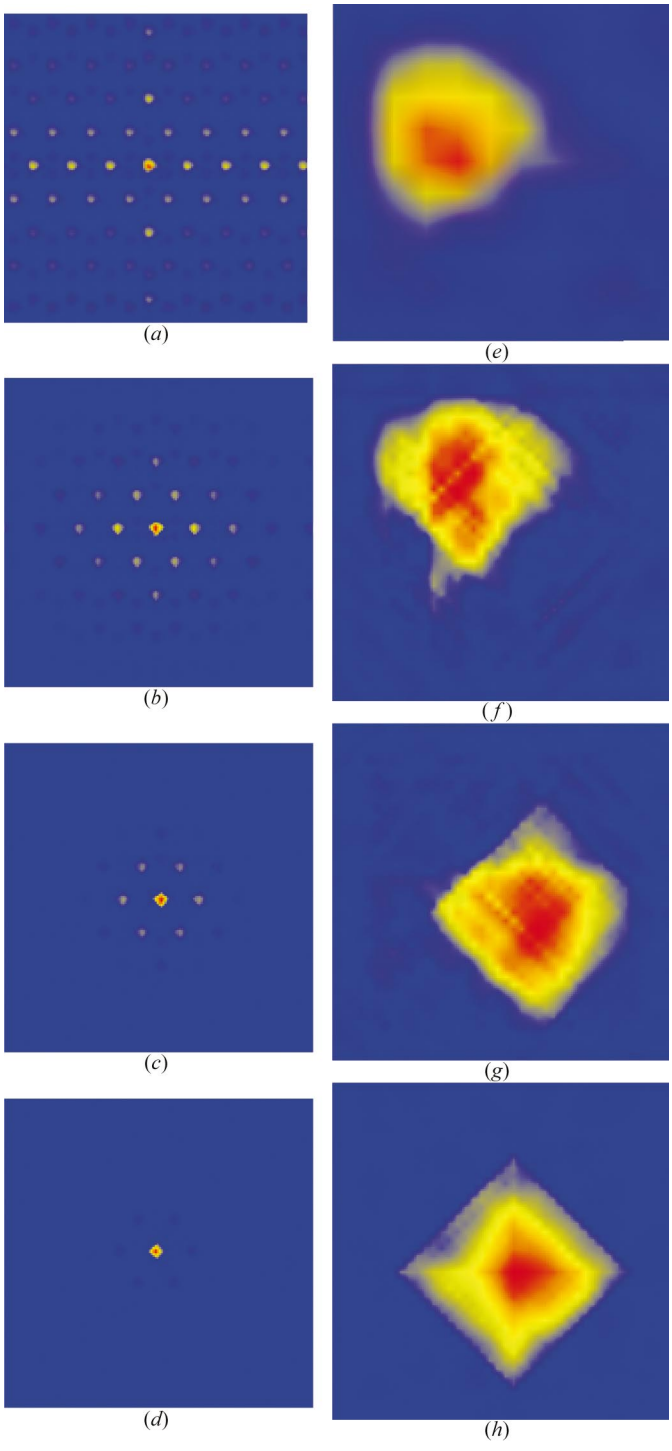

Figure 6
Reconstructed real-space images obtained from the diffraction patterns of Fig. 4 corresponding to different values of the coherence length $l_{\rm coh}$ of the incoming beam. The left-hand panel shows an image of the total array of 512 × 512 pixels. The right-hand panel shows a magnified image (40 × 40 pixels) of the central island.

Several comments are necessary here. We have demonstrated in these calculations that, contrary to common belief, even if the coherence length is reduced to the size of an individual island in the array the diffraction pattern still contains enough information to be oversampled and hence inverted. Of course, the reconstructed shape of the island can contain artifacts due to reduced coherence as discussed in a study of partial coherence effects on the imaging of single crystals (Vartanyants & Robinson, 2001, 2003).

In §2, when the array of QDs is illuminated coherently the shape of each island is reconstructed individually. At the same time, in our last example with highly reduced coherence length, it is an average shape over a number of illuminated islands that is reconstructed. In both cases, however, the result is obtained by a model-independent phase-retrieval method.

4. Conclusions

In this paper we have discussed the possibilities of imaging of quantum structures by inversion of X-ray diffraction patterns obtained with coherent and partially coherent illumination of the sample. It was shown that the diffraction pattern from a two-dimensional lattice of QDs can be inverted to give the correct shape and orientation of individual islands. For successful reconstruction, the experimental diffraction pattern has to be oversampled in a sufficient reciprocal space range $\Delta q > q_a = 2\pi/a$, where a is the average size of an island in quantum structure. The reconstructed image can occasionally be a superposition of twin images because these are both possible solutions of the inversion problem.

In this paper we limited ourselves to the case of a periodic array of identical quantum dots. Periodicity was used as an important support, shown in Fig. 2(*a*). If the initial array of QDs is non-periodic, reconstruction of the position and shape of the individual QD can become a more challenging problem. We believe that if the sample is illuminated by a finite-size coherent beam, however, the problem can be solved by oversampling and an additional 'atomicity' projection constraint proposed recently by Elser (2003). More computer calculations will be necessary to test these ideas.

We discussed the situation when the individual particles are totally relaxed. It is known, however, that often QDs have a complicated internal strain profile induced by the substrate crystal (Kegel *et al.*, 2001). This strain will reveal itself in the diffraction experiment by breaking the symmetry of the diffraction pattern (Robinson & Vartanyants, 2001). We believe that by applying a similar iteration algorithm, as discussed in this paper, the strain profile can also be reconstructed successfully once the shape of the QDs is known (Vartanyants *et al.*, 2000).

We also tested Szöke's idea of working in the extreme incoherent limit (Szöke, 2001). The correct shape of the particle can be obtained when the transverse coherence length of the incoming beam becomes of the order of the individual particle size, $l_{\rm coh} \simeq a$.

We hope that these ideas will be tested on real arrays of QDs in the near future. All parameters needed to achieve a successful reconstruction can be estimated directly from the data, so no further assumptions are required.

The work was supported by DOE DEFG 02-91ER45439 and NSF DMR 98-76610.

References

Bimberg, D., Grundmann, M. & Ledentsov, N. N. (1999). *Quantum Dot Heterostructures*. Chichester: Wiley.

Born, M. & Wolf, E. (1999). *Principles of Optics*, 7th ed. Cambridge University Press.

Darhuber, A. A., Schittenhelm, P., Holy, V., Roch, T., Stangl, J., Bauer, G. & Abstreiter, G. (1997). *Phys. Rev. B*, **55**, 15652–15663.

Eisele, H., Flebbe, O., Kalka, T., Preinesberger, C., Heinrichdorff, F., Krost, A., Bimberg, D. & Dähne-Prietsch, M. (1999). *Appl. Phys. Lett.* **75**, 106–108.

Elser, V. (2003). *J. Opt. Soc. Am. A*, **20**, 40–55.

Fienup, J. R. (1982). *Appl. Opt.* **21**, 2758–2769.

Fienup, J. R. & Wackerman, C. C. (1986). *J. Opt. Soc. Am. A*, **11**, 1897–1907.

Gerchberg, R. W. & Saxton, W. O. (1972). *Optik*, **35**, 237–246.

Goodman, J. W. (1985). *Statistical Optics*. New York: Wiley.

Holy, V., Pietsch, U. & Baumbach, T. (1999). *High Resolution X-ray Scattering from Thin Films and Multilayers*. Berlin: Springer.

Holy, V., Roch, T., Stangl, J., Daniel, A., Bauer, G., Metzger, T. H., Zhu, J., Brunner, K. & Abstreiter, G. (2001). *Phys. Rev. B*, **63**, 205318/1–5.

Kegel, I., Metzger, T. H., Lorke, A., Peisl, J., Stangl, J., Bauer, G. & Nordlund, K. (2001). *Phys. Rev. B*, **63**, 035318/1–13.

Lee, H., Johnson, J. A., He, N. Y., Speck, J. S. & Petroff, P. M. (2001). *Appl. Phys. Lett.* **78**, 105–107.

Lin, B., Schlossman, M. L., Meron, M., Williams, S. M., Huang, Z. & Viccaro, P. J. (1998). *Phys. Rev. B*, **58**, 8025–8037.

Liu, C.-P., Gibson, J. M., Cahgill, D. G., Kamins T. I., Basile, D. P. & Williams, R. S. (2000). *Phys. Rev. Lett.* **84**, 1958–1961.

Liu, N., Tersoff, J., Baklenov, O., Holmes, A. L. Jr & Shih, C. K. (2000). *Phys. Rev. Lett.* **84**, 334–337.

Mandel, L. & Wolf, E. (1995). *Optical Coherence and Quantum Optics*. Cambridge University Press.

Marquez, J., Geelhaar, L. & Jacobi, K. (2001). *Appl. Phys. Lett.* **78**, 2309–2311.

Mateeva, E., Sutter, P. & Lagally, M. G. (1999). *Appl. Phys. Lett.* **74**, 567–569.

Medeiros-Ribeiro, G., Bratkovsky, A. M., Kamins, T. I., Ohlberg, D. A. A. & Williams, R. S. (1998). *Science*, **279**, 353–355.

Miao, J., Charalambous, P., Kirz, J. & Sayre, D. (1999). *Nature (London)*, **400**, 342–344.

Miao, J., Ishikawa, T., Johnson, B., Andersen, E., Lai, B. & Hodgson, K. (2002). *Phys. Rev. Lett.* **89**, 088303/1–4.

Miao, J. & Sayre, D. (2000). *Acta Cryst.* A**56**, 596–605.

Miao, J., Sayre, D. & Chapman, H. N. (1998). *J. Opt. Soc. Am. A*, **15**, 1662–1669.

Millane, R. P. (1996). *J. Opt. Soc. Am. A*, **13**, 725–734.

Millane, R. P. & Stroud, W. J. (1997). *J. Opt. Soc. Am. A*, **14**, 568–579.

Robinson, I. K. & Vartanyants, I. A. (2001). *Appl. Surf. Sci.* **182**, 186–191.

Robinson, I. K., Vartanyants, I. A., Williams, G. J., Pfeifer, M. A. & Pitney, J. A. (2001). *Phys. Rev. Lett.* **87**, 195505/1–4.

Salditt, T., Rhan, H., Metzger, T. H., Peisl, J., Schuster, R. & Kotthaus, J. P. (1994). *Z. Phys. B*, **96**, 227–230.

Schmidbauer, M., Wiebach, Th., Raidt, H., Hanke, M., Köler, R. & Wawra, H. (1998). *Phys. Rev. B*, **58**, 10523–10531.

Shen, Q., Kycia, W., Tentarelli, E. S., Schaff, W. J. & Eastman, L. F. (1996). *Phys. Rev. B*, **54**, 16381–16384.

Shen, Q., Umbach, C. C., Wecelak, B. & Blakely, J. M. (1993). *Phys. Rev. B*, **48**, 17967–17971.

Springholz, G., Holy, V., Pinczolits, M. & Bauer, G. (1998). *Science*, **282**, 734–737.

Stangl, J., Holy, V., Roch, T., Daniel, A., Bauer, G., Zhu, J., Brunner, K. & Abstreiter, G. (2000). *Phys. Rev. B*, **62**, 7229–7236.

Stangl, J., Holy, V., Springholz, G., Bauer, G., Kegel, I. & Metzger, T. H. (2002). *Mater. Sci. Eng.* **19**, 349–358.

Steinfort, A. J., Scholte, P. M. L. O., Ettema, A., Tuinstra, F., Nielsen, M., Landmark, E., Smilgies, D. M., Feidnhans'l, R., Falkenberg, G., Seenhofer, L. & Johnson, R. L. (1996). *Phys. Rev. Lett.* **77**, 2009–2012.

Sutter, P. & Lagally, M. G. (1998). *Phys. Rev. Lett.* **81**, 3471–3474.

Szöke, A. (2001). *Acta Cryst.* A**57**, 586–603.

Vartanyants, I. A., Ern, C., Donner, W., Dosch, H. & Caliebe, W. (2000). *Appl. Phys. Lett.* **77**, 3929–3931.

Vartanyants, I. A. & Robinson, I. K. (2001). *J. Phys. Condens. Matter*, **13**, 10593–10611.

Vartanyants, I. A. & Robinson, I. K. (2003). *Opt. Commun.* **222**, 29–50.

Walther, T., Cullis, A. G., Norris, D. J. & Hopkinson, M. (2001). *Phys. Rev. Lett.* **86**, 2381–2384.

Wiebach, Th., Schmidbauer, M., Hanke, M., Raidt, H., Köler, R. & Wawra, H. (2000). *Phys. Rev. B*, **61**, 5571–5578.

Williams, G. J., Pfeifer, M. A., Vartanyants, I. A. & Robinson, I. K. (2003). *Phys. Rev. Lett.* **90**, 175501/1–4.

Zuo, J.-M., Vartanyants, I. A., Gao, M., Zhang, R. & Nagahara, L. A. (2003). *Science*, **300**, 1419–1421.

 Received 10 April 2003 • Accepted 4 August 2003